Journal of Materials Chemistry C

Accepted Manuscript

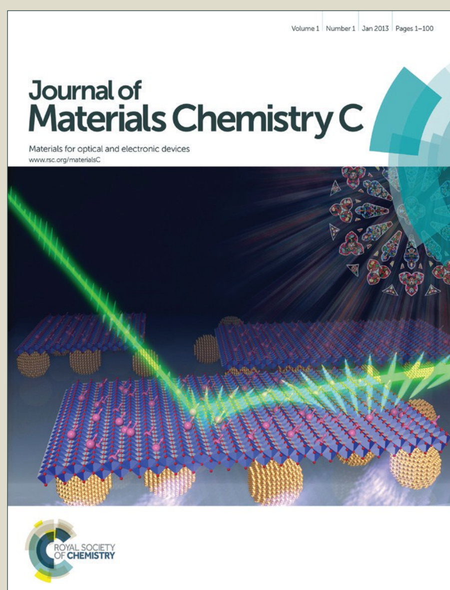

This is an *Accepted Manuscript*, which has been through the Royal Society of Chemistry peer review process and has been accepted for publication.

Accepted Manuscripts are published online shortly after acceptance, before technical editing, formatting and proof reading. Using this free service, authors can make their results available to the community, in citable form, before we publish the edited article. We will replace this *Accepted Manuscript* with the edited and formatted *Advance Article* as soon as it is available.

You can find more information about *Accepted Manuscripts* in the Information for Authors.

Please note that technical editing may introduce minor changes to the text and/or graphics, which may alter content. The journal's standard Terms & Conditions and the Ethical guidelines still apply. In no event shall the Royal Society of Chemistry be held responsible for any errors or omissions in this *Accepted Manuscript* or any consequences arising from the use of any information it contains.

ROYAL SOCIETY OF CHEMISTRY

www.rsc.org/materialsC

Journal Name RSCPublishing

ARTICLE

Flexible Inkjet Printed high-k HfO_2-Based MIM Capacitors

-Cite this: DOI: 10.1039/x0xx00000x

Received 00th January 2012,
Accepted 00th January 2012

DOI: 10.1039/x0xx00000x

www.rsc.org/

G. Vescio,[a] J. López-Vidrier,[a] R. Leghrib,[b] A. Cornet [a] and A. Cirera [a]

The soaring global demand for flexible, wearable and transparent devices has created an urgent need for new fabrication technologies that are both cost-competitive and eco-friendly. Printed electronics holds the promise of enabling low-cost, scalable solutions exploiting the ability of innovative materials to be used as processed inks onto large area substrate. In this Letter, we demonstrate the direct drop-on-demand inkjet printing technology as a viable method for fabrication of full-printed metal-insulator-metal capacitors on flexible substrate (Kapton®), where the high-k hafnium oxide (HfO_2) was selected as the dielectric. After a low-temperature annealing process, the deposited nanoparticles-based ink of HfO_2 showed high homogeneity and good integrity of the printed thin film by microscopy and spectroscopy studies. The full printed capacitors were characterized by field-emission scanning and transmission electron microscopies. X-ray diffraction patterns, as well as Raman scattering and Fourier-transform infrared spectra, revealed the presence of a polycrystalline solid layer, without solvent organic ink remains. The bonding structure of the HfO_2 layer and the interface with the Ag electrode was studied by X-ray photoelectron spectroscopy. The good performance of the thin film was proved by its relative permittivity, k = 12.6, and dielectric loss tangent, tang δ = 0.0125 at 1 MHz. Finally, the electrical current density-voltage and capacitance-voltage measurements have been studied in the frequency range 10 kHz–1 MHz. The obtained results indicate that MIM capacitors based on inkjet-printed flexible HfO_2 NPs work properly within the ITRS 2016 roadmap requirements.

1. Introduction

In recent years, printed electronics on flexible supports has quickly gained interest as a low-cost, high-area, light-weight and bendable plastic alternative to Si technology.[1-2] Amongst all the existing printing technologies, drop-on-demand inkjet printing stands out as a quick, maskless, digital-pattern design, as well as being a non-contact technique.[1,3,4] In addition, the piezoelectric cartridges used in inkjet printers, well known for their high sturdiness (no clogging nozzle), allow to print innovative materials requiring only few-picoliter amount of ink after an in-depth study of its rheology.[5,6]

Concerning the inkjet technique, drawbacks such as limited resolution and relatively large minimum thickness of the deposited layer need to be solved to obtain electronic devices with performance and reliability comparable to those based on Si technology. Therefore, complex and expensive techniques such as self-alignment printing[7,8] or femtoliter drop jetting[9] are used as advanced processes to overcome the current limitations of the inkjet printing technology. In this regard, selecting and employing outstanding materials to be printed as insulator,[10-11] such as the high-k dielectric materials[12-13] (with a higher dielectric constant than the usual SiO_2), is imperative. Furthermore, flexible and transparent substrates, which limit the temperature of the post-deposition thermal treatments down to 180 °C (Kapton® is an exception, allowing for temperatures as high as 350 °C)[14] are the most promising and suitable materials for the fabrication of bendable devices.

One of the most limiting factors for a material to be a candidate for inkjet printing is the maintenance of the physical and chemical properties of the ink when submitted to the temperatures required for the printing process. As well, the effective lifetime of the printer head must be as long as possible. To meet these requirements (thus preventing effects such as evaporation of the ink while inkjet-printing and damage to the printer head), the ink particles size must

[a] MIND-IN2UB, Electronics Departament, Universitat de Barcelona, C. Martí i Franquès 1, 08028, Barcelona, Spain. E-mail: giovescio@el.ub.edu; Tel: +34-93-4024804
[b] Laboratoire d'Electronique, de Traitement du signal et de Modélisation Physique (LETSMP) Faculté des Sciences, Université Ibn Zohr, AGADIR-
[c] †Electronic Supplementary Information (ESI) available: Details of device fabrication, XPS HfO_2 survey, C-V curves on different substrates. See DOI: 10.1039/x0xx00000x

Journal of Materials Chemistry C Accepted Manuscript

lie in the sub-micron scale (the ratio between the nanoparticle size and the printer nozzle orifice should ideally be 1/50). Nowadays, there exist very promising high-k oxides that guarantee this condition. However, for the particular application as gate oxide in MIM capacitors, other conditions have to be accomplished (thermal and kinetic stabilities, band offsets, good metal/semiconductor interface quality and low bulk defect density) apart from high dielectric constant. Among the existing high-k materials, HfO_2 and Hf silicates have been found to well fit these characteristics.[15]

During the last decade, hafnium oxide (HfO_2) has become one of the most remarkable compounds to be employed as an alternative dielectric gate due to its physical properties, such as a relative wide band gap of 5.8 eV[16] that ensures a barrier for electrical conduction at room temperature, and its higher dielectric constant (k = 20)[16] compared to SiO_2 (k = 3.9). Moreover, it is also appreciated for its hardness, high melting point, chemical resistance, resistance to impurity diffusion because of its high density (9.68 g/cm^3), and thermal stability up to 700 °C.[17,18] Finally, HfO_2 is one of the most studied materials to be implemented as optical components due to its transparency from the infrared to ultraviolet range.[19] For these reasons, HfO_2 is an attractive high-k dielectric material for the future generation of metal-oxide-semiconductor field-effect transistors (MOSFETs), micro-electro-mechanical systems (MEMS), complementary metal–oxide–silicon (CMOS) transistors, highly-scaled memories, radio frequency circuits, and a variety of configurations in analogue integrated circuits.[20]

Various methods for preparing metal oxide films have been reported, such as sputtering,[21] atomic layer deposition (ALD),[22-23] physical vapour deposition (PVD),[24] metal organic chemical vapour deposition (MOCVD),[25,26] pulsed laser deposition (PLD),[27,28] thermal evaporation,[29] sol-gel spin-coating,[14] or by sonochemistry.[30] Alongside all these methods, inkjet printing appears as a disrupting new technology that allows to selectively deposit smooth films of nanoparticles (NPs) in a non-contact process on flexible substrates for metal-insulator-metal (MIM) devices, at room temperature and ambient pressure. Consequently, lithography, etching, vacuum systems and high-temperature thermal processes are avoided.

In this study, we report the properties of HfO_2 NPs used as dielectric thin film of a full MIM capacitor. The films have been deposited on a flexible polyimide substrate by inkjet printing, followed by a low-temperature post-annealing process. To determine the insulator properties, the structure and the morphology of the film have been investigated. The morphology and the microscopic properties of the HfO_2 have been characterized by transmission electron microscopy (TEM), focused ion beam (FIB)-assisted field-emission scanning electron microscopy (FE-SEM), X-ray diffraction (XRD), Raman scattering and Fourier-Transform infrared (FTIR) spectroscopies, X-ray photoelectron spectroscopy (XPS), and UV–visible absorption spectroscopy. Device performance and reliability were tested by capacitance-voltage (C–V), and the leakage current density-voltage (J–V) characteristic was evaluated.

2. Experimental

2.1 Materials and fabrication

Ag/HfO_2/Ag MIM capacitors were printed onto polyamide Kapton® flexible substrate with a Xennia XenJet 4000 inkjet printing system, using Xaar cartridges (XJ126-50 series), with an ink droplet volume fixed at 50 pl. For the electrodes and the dielectric layer, Ag nanoparticle-based ink U5603 from Sun Chemical Corporation and HfO_2 NPs ink from Torrecid S.A. were used, respectively.

The HfO_2 NPs were synthesized by means of spray-pyrolysis from hafnium acetylacetonate dissolved in aliphatic compounds. The ink was prepared by dispersing HfO_2 nanoparticles in the liquid vehicle formed by solvents and other additives by using the following approximate formula in the Table 1.

Table 1. Hafnium oxide ink compounds.

Component	*wt %*
HfO_2	*45 - 50*
Mixed aliphatic compounds	*42 - 47*
Organic hydroxy compounds	*5 - 8*
Polymeric amide derivatives	*2 - 4*
Polymethylsiloxane derivative	*0.05 – 0.1*
Modified amide derivative	*0.1 –0.3*
Organic thixotropic agents	*0.1 – 0.2*

Prior to the printing process, standard cleaning of the Kapton® surface substrate was carried out. A silver bottom electrode with a thickness of 300 nm was printed; afterwards, it was annealed at 220 °C for 20 minutes in order to remove the organic solvents and to achieve a resistivity around 16 μΩ·cm, which is among the best values found in the literature.[31]

For the HfO_2 deposition onto the bottom electrode, an ink ejection frequency of 7.5 kHz and a resolution of 450 drops per inch (DPI) between the ink droplets were used. During the HfO_2 layer printing, the substrate temperature was kept constant at 55 °C in order to attain a proper adhesion between the different layers. To reach a more homogeneous layer, which implies a better dielectric behaviour, a post-deposition annealing at 250 °C for 180 minutes was performed, according to the results of thermogravity analysis (TGA) [see Fig. S1 in the Supplementary Data] and differential scanning calorimetry (DSC) [Fig. S2]. Subsequently, the silver NPs top electrode was deposited under the same printing conditions than the bottom electrode and annealed at 220 °C for 20 minutes. In order to enhance contrast resolution in FIB-processed FESEM-images, a bottom contact of sputtered Pt was used.

Finally, a layer of PMMA was deposited by drop coating on the fabricated devices to protect them from any environmental contamination. Fig. 1 shows the scheme and the photo of the printed MIM structure under study.

Journal of Materials Chemistry C Accepted Manuscript

This journal is © The Royal Society of Chemistry 2012

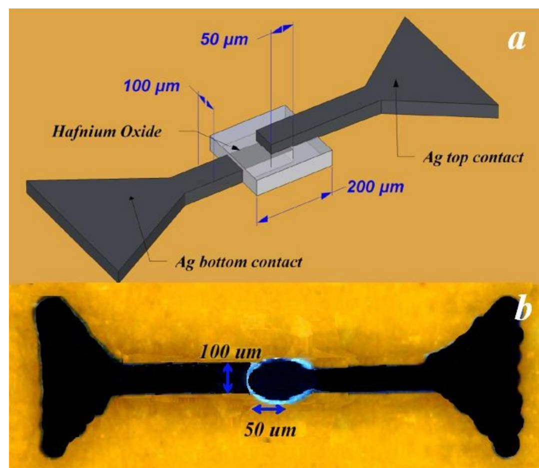

Fig. 1 (a) Scheme of the MIM structure under study. (b) Microscopy image of an Ag/HfO_2/Ag (MIM) capacitor, printed by inkjet printing technique.

2.2 Structural and physicochemical characterization

Inkjet-printed HfO_2 thin films were characterized morphologically, structurally and chemically.

The morphology and structure of the inkjet-printed MIM Ag/HfO_2/Ag devices were studied by FE-SEM with a FEI Nova 200 instrument, and by TEM using a JEOL JEM 2100 microscope. FE-SEM cross-section samples were cut with FIB (FEI dual beam STRATA 235). The surface roughness was evaluated using an AFM Digital Instruments Nanoscope D-5000. The morphology of the sample surface was accurately observed by scanning the x-y plane, with a z-axis resolution limit around ~1 nm.

The crystalline microstructure, orientation and size of the HfO_2 NPs were studied by XRD using a Japan Rigaku D/Max-IIA X-ray diffractometer using Cu K_α radiation, λ = 1.5406 Å, operating at 40 keV and 40 mA. A further study of the HfO_2 layer crystallinity and vibration properties was performed by means of Raman scattering, employing a Horiba Jobin-Yvon LabRam HR800 micro-Raman spectrometer operating at 20 mW laser power and an excitation wavelength of 532 nm (2nd harmonic of a Nd:YAG laser).

The analysis of the chemical composition of the HfO_2 thin film was performed using a PHI ESCA-5500 X-ray photoelectron spectrometer with a monochromatic Al K_α radiation (E = 1486 eV) at 350.0 W with the X-ray source and detector forming an angle of 45° with the normal of the sample, i.e. 90° between them. Additionally, a Thermo Scientific Systems NICOLET iN10 FT-IR spectrometer with a DTGS detector for far-IR in the range from 4000 to 220 cm^{-1} was used to study the presence of the different remaining compounds adsorbed on the HfO_2 surface.

The thickness of the HfO_2 layers was estimated using the NanoSpec® 6100 Automated Film Thickness (AFT) Measurement System, whereas UV–Vis spectroscopy analysis was carried out by means of a Hewlett Packard HP-8453 spectrophotometer to determine the optical properties of the material.

The current versus DC voltage characteristics were measured by means of a Keithley 4200-SCS Semiconductor Characterization System. The admittance versus voltage and admittance versus frequency curves were obtained using the same Keithley 4200-SCS with the integrated C–V (capacitance-voltage) instrument for frequencies from 10 kHz to 1 MHz and DC voltage biases in the range from -5 to +5 V.

3. Results

3.1 Thin film morphology

The morphology and shape of the as-printed dielectric layer was analyzed, thus the overall thin film structure was surveyed in depth. Fig. 2(a) shows a TEM image of the HfO_2 NPs film where the sample appears as a series of nanoparticles embedded within a polycrystalline matrix. We can observe how the HfO_2 NPs are sphere-shaped, being the estimated regular diameter of NPs around 25 nm (Figure 2(b)). Besides, the selected area electron diffraction analysis of the HfO_2 shows that NPs are polycrystalline with a lattice spacing of ~2.2 Å, in agreement with the monoclinic phase structure.[32]

In order to examine the surface of the printed layer, an AFM study was carried out. Fig. 3 presents a top-view AFM image of the HfO_2 films deposited by the inkjet technique process, after being sintered at 250 °C. The layer exhibits an RMS roughness value lower than 25 nm, which suggests compact NPs disposition into the layer, taking in account the grain size of these NPs.

As reported by other authors, a homogeneous and smooth surface is required for the fabrication of bottom-gate devices where even moderate interface roughness can adversely affect the material properties, such as carrier mobility.[33,34] In the case of the inkjet-printed MIM capacitors presented in this work, roughness is only related, in the best cases, to the NPs size. However, a further drawback could appear considering the propagation of surface

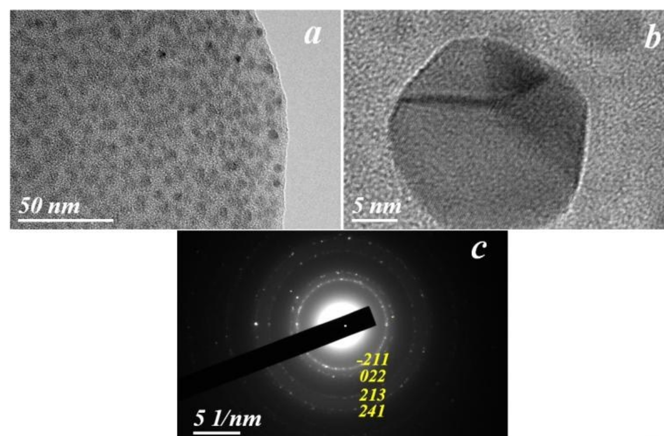

Fig. 2 (a),(b) TEM images of HfO_2 thin film annealed at 250 °C for 2h deposited on Ag bottom contact films. (c) Selected area electron diffraction showing pattern rings of the HfO_2 NPs.

Journal of Materials Chemistry C Accepted Manuscript

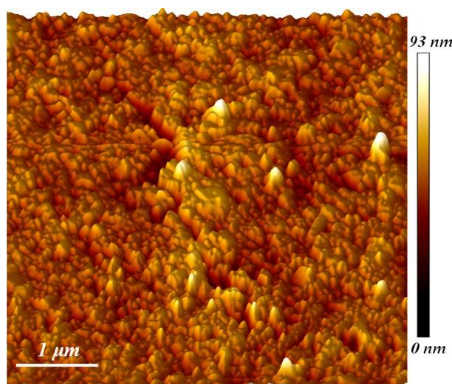

Fig. 3 HfO_2 films on Ag bottom contact on Kapton® flexible substrate. Top-view AFM 3D image of an area of 5 × 5 µm^2.

defects (mainly pinholes) through the layer (in depth), which can induce a short circuit. For this purpose, we analyzed the device cross-section by FIB-assisted FE-SEM, as shown in Fig. 4. The section profile of the inkjet-printed HfO_2 film shows a good homogeneity and the integrity of the layers, with a thickness around 400 nm. Moreover, the whole MIM capacitor section on the substrate does not show any propagation of printing errors or large cavities among the layers. Additionally, the spectroscopic reflectometry results proved the fine control deposition achieved by a single printing process. The thickness of the HfO_2 thin film layer was measured to be around 100 nm, in agreement with the FIB cross-section image in Fig. S3.

Finally, SEM cross-section image demonstrated that the film was grown quite uniformly over the metal film surface, following the roughness of the substrate surface. The possible porosity is still not well understood; therefore, further studies are required.

Overall, the structural characterization has shown that the morphology of the printed dielectric layer evidences a solid and stable structure without detrimental wrinkles, fractures or pin-holes.

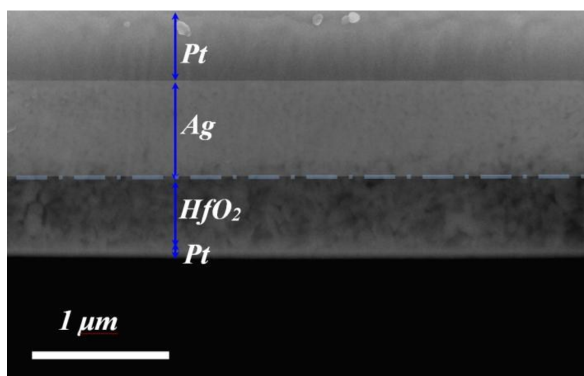

Fig. 4 Cross-section of MIM capacitor by FIB-assisted FE-SEM technique. The layers have a Pt bottom electrode thickness of 50 nm, 400 nm for HfO_2 and 700 nm of Ag top contact.

3.2 Crystalline structure

The crystalline structure, size and orientation of the HfO_2 thin films were investigated by XRD, the results being shown in Fig. 5. The XRD pattern clearly shows the characteristic reflections of the HfO_2 monoclinic phase labelled by the circle symbol, as expected from the nature of the nanoparticles. The printed layer principally exhibited polycrystalline monoclinic structure and mainly revealed (and (111) reflections (PDF#078-0049) at 28.16° and 31.85°, respectively.[35] Monoclinic HfO_2 phase is the most stable and well-studied structure according to the experimental and theoretical investigations in the previously reported works at low temperature.[36,37] No other phases were observed, nor phenomena related to the nanoparticles recrystallization during the thermal annealing processes. In particular, the specimens evidenced the absence of the characteristic peak at 30.3° of metastable cubic, tetragonal, or orthorhombic phases of HfO_2.[38-39]

The XRD peaks centred at 2θ = 27.80°, 32.18°, and 46.26° indicate the presence of a crystalline phase of Ag-4,4'-dimethyldiazoaminobenzene ($C_{14}H_{14}AgN_3$).[40] In our case, $C_{14}H_{14}AgN_3$ forms from the Ag bottom contact; however, it does not affect the crystalline structure as proved by the clearly identifiable HfO_2 peaks (monoclinic phase) in the XRD patterns in the Fig. 5.

The size of HfO_2 NPs was estimated from the full-width at half-maximum (FWHM) of the XRD reflection according to the Debye–Scherrer's equation (eq. 1).[41] Considering the peak at different degrees, the average particle size, *D*, has been evaluated according to:

$$D = (0.9\,\lambda) / [\beta \cos(\vartheta)] \qquad (1)$$

where $\lambda = 0.15406$ nm is the wavelength of X-ray radiation, β is the full-width at half-maximum (FWHM) and θ is the diffraction angle.

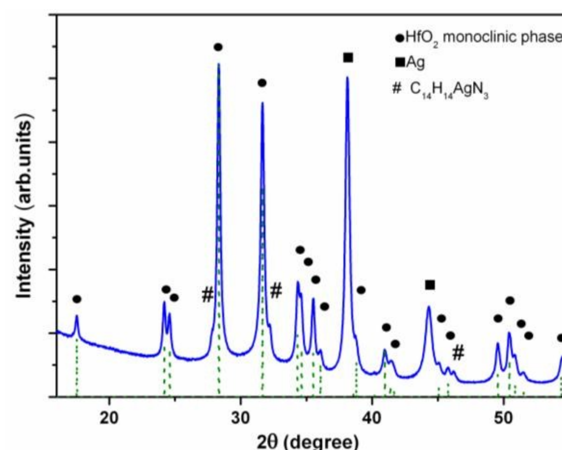

Fig. 5 XRD pattern of 120-nm thick HfO_2 annealed at 250 °C, deposited on a Ag bottom contact layer of 300nm. Ag and main monoclinic HfO_2 peaks are labelled.

Journal of Materials Chemistry C Accepted Manuscript

This journal is © The Royal Society of Chemistry 2012

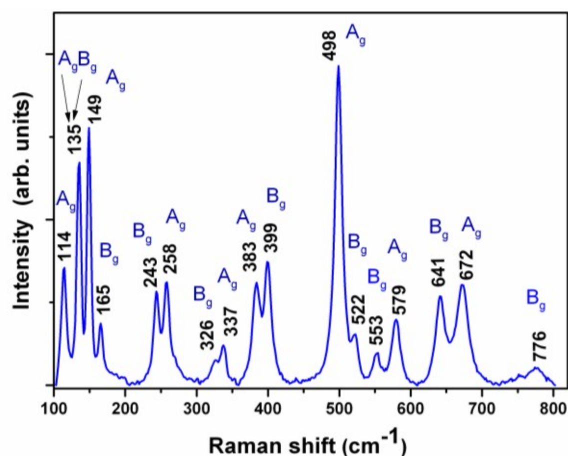

Fig. 6 Raman spectrum of the printed HfO_2. Monoclinic vibration modes of HfO_2 are labelled. The vibration modes are classified into A_g and B_g mode.

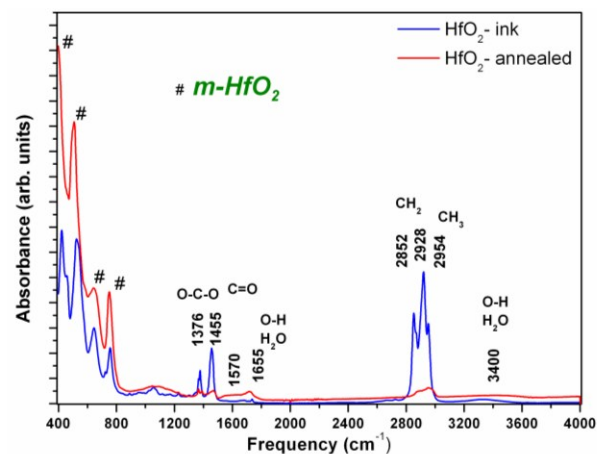

Fig. 7 FT-IR spectra comparison between HfO_2 ink compound and HfO_2-annealed sample at 250 °C.

The average crystallite size of the as-prepared HfO_2 NPs was calculated to be around 25 nm, in agreement with the size calculated previously from TEM images, like in previous works in the literature.[42-43]

The crystalline quality, uniformity and purity of HfO_2 NPs thin film were investigated also by micro-Raman analysis in the Fig. 6. The Raman spectra were referenced to crystalline silicon main vibration at 521 cm^{-1}. The data were acquired in the spectral region from 100 to 800 cm^{-1}. The Raman spectrum of the HfO_2 oxide is shown in Figure 6, where the monoclinic phase of HfO_2 exhibits two Raman-active in-phase vibration modes, A_g and B_g. Only 18 active vibration modes are expected in the Raman spectra of HfO_2 ($9A_g$+$9B_g$) as confirmed from the spectra. These peaks are in good agreement with allowed phonon modes predicted for the HfO_2 monoclinic phase in the range from 100 to 800 cm^{-1}.[44-45]

The presence of remaining carbon contamination was analyzed by FT-IR. The acquired spectra are displayed in Fig. 7, where the peaks associated with the HfO_2 monoclinic phase (red line) are represented in the range from 4000 to 400 cm^{-1}. The main absorption bands in the infrared region are placed at 418, 514, 763 and 647 cm^{-1};[46,47] all of them are ascribed to the monoclinic hafnium oxide (m-HfO_2) phonon bands, in good agreement with previously reported values.[37,48,49,50,51] FT-IR measurements allowed us to identify any possible adsorbed contaminants by other absorption peaks in the range of 3400–1300 cm^{-1} where the peaks are attributed to the H-bonded OH group of water, carbon bonding and to the bonding mode (H–O–H) of the water molecules.[46,48,52-53]

In fact, carbon compounds could be attributed to the inkjet process, and more precisely to an ink hydrocarbon vehicle. In Fig. 7 we show the characteristic FT-IR spectrum of the HfO_2 ink compound in the liquid phase (in blue) in comparison with the HfO_2 annealed layer (in red). Then, we can observe that the peaks of the vehicle fade out after the sintering process.

It should be noticed that residual organic carbon could affect the electrical properties of the insulator, which it clearly seems one of the causes of the reduction of the expected dielectric constant of the material. Furthermore, this undesired residual carbon will probably enhance the conductivity of the layer by means of trapped charges into the high-k layer.

It is indispensable to explore and consider the stoichiometry of the HfO_2 and the relation of carbon compounds into the printed layer in order to watch over and guarantee an ideal insulator without trapped charges. For this purpose, Fig. 8(a) shows the XPS multiplex spectra of the HfO_2 layer. The wide energy survey spectrum exhibited the distinctive peaks of HfO_2 bonds, with their corresponding binding energies (BE). An analysis of these peaks revealed that 212.6 and 223.3 eV correspond to the $4d_{5/2}$ and $4d_{3/2}$ doublet of the Hf 4d spin-orbit doublet characteristic of HfO_2. The characteristic peak of the Hf 4p photoelectron line is located at the binding energy of 381.4 eV ($4p_{3/2}$), which corresponds to HfO_2.[54,55] The presence of the C 1s peak at 284.8 eV was attributed to the adsorbed carbon from the environment, the adventitious carbon [56-57-58] [Fig. S4]. It should be mentioned that, at the interface of the structure HfO_2/Ag bottom contact [see Fig. S5] a feeble carbon peak can be observed. Since the analysis of this contribution is not in the scope of the present study, its consequences on the electrical transport and charge trapping phenomena will be evaluated in a future work.

Details of Hf 4f spectrum are shown in Fig. 8(b). The asymmetric shape of the spectrum suggests the presence of smaller doublet peaks, each with an 1.68 eV separation, towards lower BE for the expected Hf–O bonds. Therefore the Hf 4f energy level region can be deconvolved into three spin-orbit doublet peaks with the corresponding $4f_{7/2}$ binding energies at 15.4, 15.8, and 17.1 eV. In accordance to previous studies, the first two doublets exhibit larger widths than 0.9 eV and can accordingly be assigned to a Hf^{x+} suboxide, whereas the last one can be ascribed to the fully oxidized hafnium (Hf^{4+}).[17,59,60-61]

Journal of Materials Chemistry C Accepted Manuscript

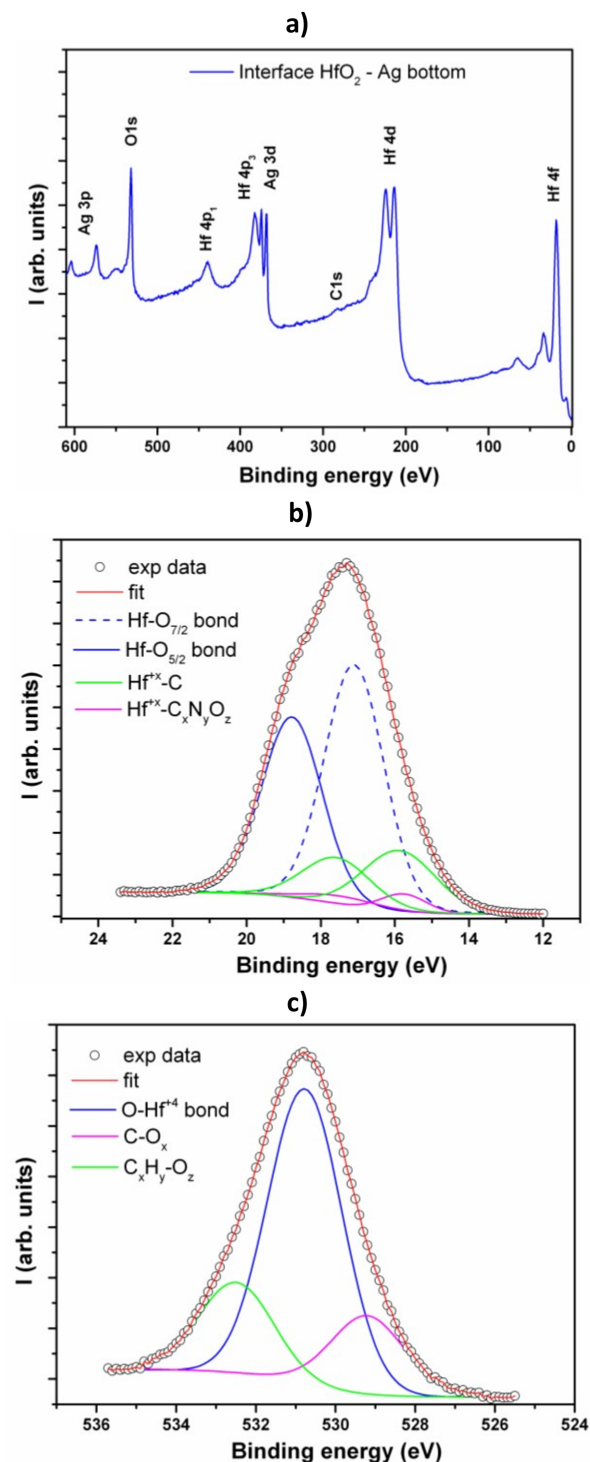

Fig. 8 (a) XPS Binding energy survey and (b, c) high-resolution XPS spectra of Hf and O in annealed HfO_2 thin film at 250 °C for 3 h, deposited on Ag bottom contact. The curves represent the experimental data with the fit of the corresponding peaks.

The formation of the suboxide probably depends on the substrate temperature and the depositing conditions that may induce bond structures such as HfOC,[62] or $HfC_xN_yO_z$,[63,64] as indicated by the O 1s spectra in Fig. 8(c). The peak placed at 530.7 eV (O 1s) is attributed to (metal-oxygen) Hf–O bonds, whereas the peaks at 529.1 and 532.5 eV indicate bond structures such as CO_x (adventitious carbon)[56] or $C_xH_yO_z$.[59,65,66] Nevertheless, their low relative intensity suggests a low concentration of these bonds, as confirmed by the FT-IR study.

In conclusion, the effective stoichiometry O:Hf could be estimated around 1.85, a good value that confirms, despite the dielectric thickness, how reliable the inkjet technology is in terms of purity in comparison to other well-known small-area and expensive technologies such as sputtering, ALD or CVD.[21,25,26,67]

3.3 Optical and electrical properties

The absorption spectrum of the HfO_2 NPs ink was acquired within the UV-vis range to evaluate the optical properties of the dielectric. The absorbance spectra recorded in the region from 190 to 1100 nm (see the inset in Fig. 9) allowed us estimating the energy band gap (E_g) value of the HfO_2 NPs. This was achieved considering the Tauc law, able to fit the absorption coefficient in both direct and indirect band gap semiconductors[68] by plotting $(\gamma h\nu)^2$ versus photon energy ($h\nu$), using (eq. 2):

(2)

where is the absorption coefficient, A is a constant, and E_g is the optical band gap of the NPs-based material. Looking at the fit in Fig. 9, we can conclude that the film presents a direct band gap, whose energy value can be obtained from the fit intersection with the photon energy axis. The image shows the derived value of the energy band gap, being E_g = 5.37 eV, which is found to be close to the previously reported value for polycrystalline HfO_2 NPs film.[69,70]

In order to characterize the electrical properties of the high-k HfO_2 NPs thin film, C–V measurements were carried out in the frequency range from 10 kHz to 1 MHz [Fig. S6]. From the voltage dependence of capacitance characteristic, the voltage coefficients of capacitance (VCCs) have been evaluated, which can be fitted by means of the following polynomial relation (eq. 3):[71]

$$C_p=C_0\,(\alpha\cdot V^2+\beta\cdot V+1) \qquad (3)$$

where C_0 is the capacitance value at zero bias voltage, and α and β are the quadratic and linear voltage dependences, respectively.[71] According to the ITRS roadmap up to 2016,[72] the quadratic coefficient of capacitance α might be smaller than 100 ppm/V^2, whereas β should lie below ±1000 ppm/V, for frequencies above 100 kHz. The obtained VCC values from the C–V measurements are shown in the Table 2. It can be seen that the smallest α and β values are measured at higher frequencies, which can be explained as a result of the slow time constant of traps within the HfO_2-related dielectrics.[73]

Journal of Materials Chemistry C Accepted Manuscript

This journal is © The Royal Society of Chemistry 2012

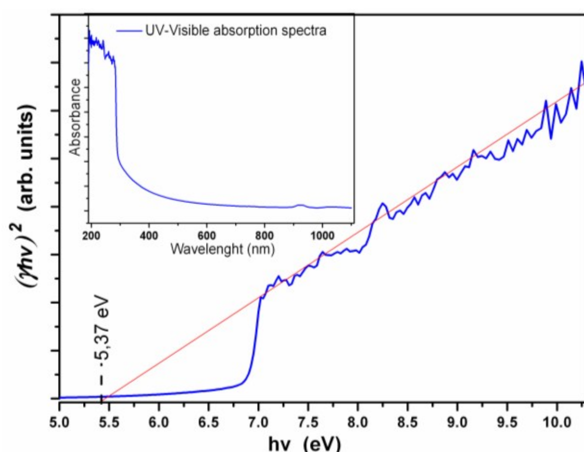

Fig. 9 Tauc plot fit corresponding to the UV-visible absorbance spectra of HfO_2 films which is displayed in the inset.

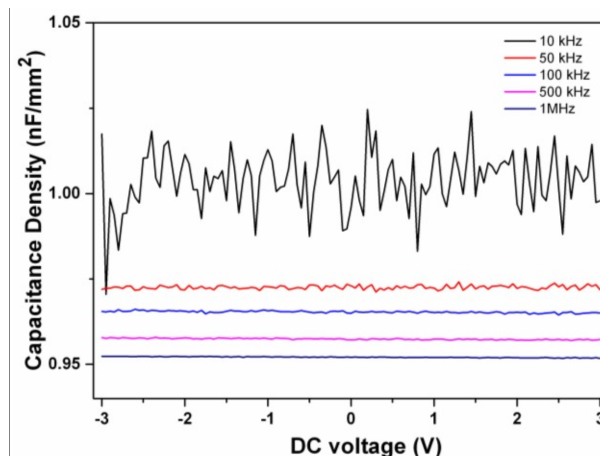

Fig. 10 Capacitance density at different frequencies.

In order to understand the behaviour of *α* and *β* with frequency, we can consider that for analogue-circuit applications the *α* parameter is the most important value, as *β* value can be compensated by custom circuit design. Therefore, the interest is focused on the nonlinear behaviour of the standard C–V curves. The quadratic voltage characteristic is attributed to the following relation (eq. 4):[74,75]

$$\alpha = 2(n_2 \cdot n_0)/(d^2 \cdot k_{lin}) \qquad (4)$$

where n_0 is the linear refractive index, k_{lin} is the linear dielectric constant, n_2 is the nonlinear refractive index that contemplates the elastic properties of the oxide, and *d* the thickness of the dielectric layer. The high-k MIM capacitors exhibit a strong positive parabola [Fig. S6], probably due to a high degree of electric field polarization and carrier injection.[24,76,77] The quadratic voltage coefficient of capacitance decreases with the applied frequency due to the change of relaxation time with different carrier mobility within the insulator, and correlates with the dielectric composition and thickness, which is an intrinsic property owing to the electric field polarization.[28,74]

From capacitance values, assuming plane-parallel electrodes, the obtained relative permittivity was k = 12.6 ± 0.8 at 1 MHz [see Figs. S7 and S8]. This value is perfectly comparable with the value of previous works[16] and it demonstrates that inkjet printing of high-k HfO_2 is a reliable technology towards high-quality device fabrication. Fig. 10 shows the capacitance density at different frequencies, exhibiting a constant value in the range around ±3V.

Table 2. Quadratic and linear voltage coefficients of capacitance (VCCs) at different frequencies, corresponding to a 400-nm-thick MIM capacitor.

HfO_2 MIM capacitor 400-nm thick

Frequency	α (ppm/V²)	β (ppm/V)
10 kHz	*452*	*-6490*
100 kHz	*109*	*-920*
1 MHz	*18*	*146*

The plot in Fig. 11 shows the leakage current density-voltage characteristics of HfO_2 MIM capacitor for a 400-nm-thick oxide film. The *J–V* characteristic was measured from an area of 2×10^{-4} cm^2 for all samples. Particularly, lower leakage currents of ~3×10^{-7} A/cm^2 at ±3 V were obtained.

Finally, the loss tangent value (1/*Q* factor) was determined as a function of frequency for the HfO_2 dielectric MIM capacitors. Fig. 12 showed similar trend in the loss tangent values for all the samples, exhibiting a value around 0.0125 at a frequency of 1 MHz,[72] well below the ITRS roadmap scheduled data for 2016 (horizontal dotted line).

In the light of the all above-mentioned studies, inkjet printing is demonstrated as a promising technology that allows selectively depositing, in a non-contact process and at ambient pressure, reliable thin films of the outstanding high-k dielectric HfO_2 on flexible substrates for MIM devices.

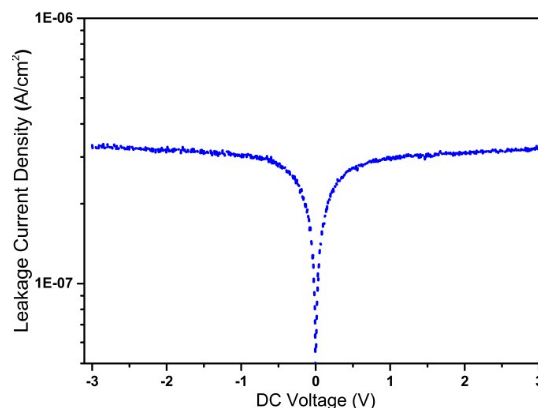

Fig. 11 Leakage current density-voltage characteristics of MIM capacitor formed by an inkjet-printed 400-nm-thick HfO_2 thin film.

Journal of Materials Chemistry C Accepted Manuscript

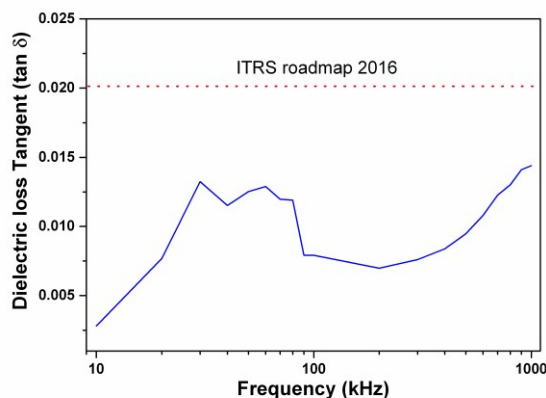

Fig. 12 Plot of the dielectric loss tangent value of a MIM capacitor ($Ag/HfO_2/Ag$ structure) deposited by inkjet printing technique.

Conclusions

Fully-printed flexible HfO_2-based MIM capacitors were fabricated by inkjet-printing followed by a low-temperature thermal treatment. Ag ink was printed to form both top and bottom electrodes, whereas HfO_2 NPs ink was used to print the high-k dielectric thin film. FE-SEM and TEM images revealed the homogeneity of the insulating layer with spherical-shaped NPs of 25 nm diameter. A uniform polycrystalline structure with good purity was confirmed from XRD, FTIR and Raman scattering studies. The optical band gap energy was determined to be 5.37 eV by UV-Vis absorption spectroscopy.

The HfO_2 thin film oxide exhibits relative permittivity and dielectric loss tangent of k=12.6 and tang δ=0.0125 at 1 MHz, respectively. Below breakdown voltages, the leakage current did not exceed 6×10^{-8} A/cm^2 at +3 V and ~3×10^{-7} A/cm^2 at -3 V. The general stability and repeatability of the dielectric properties were confirmed by the VCCs coefficients (*α* and *β),* which behave as established by the ITRS roadmap, even at frequencies as high as 1 MHz.

Further work is required to reduce HfO_2 layer thickness in order to be comparable with those of silicon- and glass-based capacitor devices in the near future.

To sum up, all the parameters obtained from the structural, optical and electrical studies carried out in this work indicate that inkjet-printed flexible HfO_2 NPs–based MIM capacitors are suitable candidates to become a possible alternative to Si-based devices in the next future. Simultaneously, the demand for an innovative transparent, flexible and reliable technology is increasing due to the possibility of being employed in emerging fields such as biological sensors and flexible systems. For such applications, low-cost production and device integration are the key requirements, which can be provided by the promising inkjet printing technology.

Acknowledgements

G. Vescio acknowledges the Spanish Government for his PhD grant in the FPU program. A. Cirera acknowledges support from 2015 edition of BBVA Foundation Grants for Researchers and Cultural Creators.

References

1. H. Y. Tseng and V. Subramanian, *Org. Electron. physics, Mater. Appl.*, 2011, **12**, 249–256.
2. M. Caironi, E. Gili, T. Sakanoue, X. Cheng, and H. Sirringhaus, *ACS Nano*, 2010, **4**, 1451–1456.
3. R. M. Verkouteren and J. R. Verkouteren, *Langmuir*, 2011, **27**, 9644–53.
4. H. Sirringhaus, T. Kawase, R. H. Friend, T. Shimoda, M. Inbasekaran, W. Wu, and E. P. Woo, *Science*, 2000, **290**, 2123–2126.
5. Shlomo Magdassi and S. Magdassi, *Pigment Resin Technol.*, 1987, 16, 4–10.
6. H. Minemawari, T. Yamada, H. Matsui, J. Tsutsumi, S. Haas, R. Chiba, R. Kumai, and T. Hasegawa, *Nature*, 2011, **475**, 364–367.
7. C. Wang, J.-C. Chien, H. Fang, K. Takei, J. Nah, E. Plis, S. Krishna, A. M. Niknejad, and A. Javey, *Nano Lett.*, 2012, **12**, 4140–5.
8. N. Zhao, M. Chiesa, H. Sirringhaus, Y. Li, Y. Wu, and B. Ong, *J. Appl. Phys.*, 2007, **101**, 064513.
9. T. Sekitani, Y. Noguchi, U. Zschieschang, H. Klauk, and T. Someya, *Proc. Natl. Acad. Sci. U. S. A.*, 2008, **105**, 4976–4980.
10. C. Mariotti, S. Member, B. S. Cook, L. Roselli, S. Member, and M. M. Tentzeris, *Ieee Microw. Wirel. Components Lett.*, 2015, **25**, 13–15.
11. B. S. Cook, J. R. Cooper, and M. M. Tentzeris, *IEEE Microw. Wirel. Components Lett.*, 2013, **23**, 353–355.
12. B. Miao, R. Mahapatra, N. Wright, and A. Horsfall, *J. Appl. Phys.*, 2008, **104**, 054510.

Journal of Materials Chemistry C Accepted Manuscript

 This journal is © The Royal Society of Chemistry 2012

13. S.-J. Ding, C. Zhu, M.-F. Li, and D. W. Zhang, *Appl. Phys. Lett.*, 2005, **87**, 053501.

14. J. S. Meena, M.-C. Chu, S.-W. Kuo, F.-C. Chang, and F.-H. Ko, *Phys. Chem. Chem. Phys.*, 2010, **12**, 2582–9.

15. J. Robertson and R. M. Wallace, *Mater. Sci. Eng. R*, 2015, **88**, 1–41.

16. J. Robertson, *Eur. Phys. J. Appl. Phys.*, 2004, **291**, 265–291.

17. S. Suzer, S. Sayan, M. M. Banaszak Holl, E. Garfunkel, Z. Hussain, and N. M. Hamdan, *J. Vac. Sci. Technol. A Vacuum, Surfaces, Film.*, 2003, **21**, 106.

18. O. Khaldi, P. Gonon, C. Mannequin, C. Vallee, F. Jomni, and a. Sylvestre, *ECS Solid State Lett.*, 2013, **2**, N15–N17.

19. T. Tan, Z. Liu, H. Lu, W. Liu, and H. Tian, *Opt. Mater. (Amst).*, 2010, **32**, 432–435.

20. J. Y. Soon and Y. Roh, *2006 IEEE Nanotechnol. Mater. Devices Conf.*, 2006, 546–547.

21. F. L. Martínez, M. Toledano-Luque, J. J. Gandía, J. Cárabe, W. Bohne, J. Röhrich, E. Strub, and I. Mártil, *J. Phys. D. Appl. Phys.*, 2007, **40**, 5256–5265.

22. rsta, and M. Les , *J. Electrochem. Soc.*, 2005, **152**, F75.

23. X. Yu, C. Zhu, H. Hu, and A. Chin, *IEEE ELECTRON DEVICE Lett.*, 2003, **24**, 63–65.

24. S. J. Kim, B. J. Cho, M. F. Li, X. Yu, C. Zhu, A. Chin, and D. Kwong, *IEEE ELECTRON DEVICE Lett.*, 2003, **24**, 387–389.

25. N. V. Nguyen, A. V. Davydov, D. Chandler-Horowitz, and M. M. Frank, *Appl. Phys. Lett.*, 2005, **87**, 192903.

26. J. Park, B. K. Park, M. Cho, C. S. Hwang, K. Oh, and D. Y. Yang, *J. Electrochem. Soc.*, 2002, **149**, G89–G94.

27. M. Ratzke, D. Wolfframm, M. Kappa, S. Kouteva-Arguirova, and J. Reif, *Appl. Surf. Sci.*, 2005, **247**, 128–133.

28. H. Hu, C. Zhu, Y. F. Lu, Y. H. Wu, T. Liew, M. F. Li, B. J. Cho, W. K. Choi, and N. Yakovlev, *J. Appl. Phys.*, 2003, **94**, 551.

29. R. Garg, N. a. Chowdhury, M. Bhaskaran, P. K. Swain, and D. Misra, *J. Electrochem. Soc.*, 2004, **151**, F215.

30. A. Ramadoss and S. J. Kim, *J. Alloys Compd.*, 2012, **544**, 115–119.

31. B. J. Perelaer, A. W. M. de Laat, C. E. Hendriks, and U. S. Schubert, *J. Mater. Chem.*, 2008, **18**, 3209.

32. A. Mukhopadhyay, J. Sanz, and C. Musgrave, *Phys. Rev. B*, 2006, **73**, 115330.

33. J. R. Williams, T. Low, M. S. Lundstrom, and C. M. Marcus, *Nat. Nanotechnol.*, 2011, **6**, 222–5.

34. K. Everaerts, J. D. Emery, D. Jariwala, H. J. Karmel, V. K. Sangwan, P. L. Prabhumirashi, M. L. Geier, J. J. McMorrow, M. J. Bedzyk, A. Facchetti, M. C. Hersam, and T. J. Marks, *J. Am. Chem. Soc.*, 2013, **135**, 8926–39.

35. R. E. Hann, P. R. Suitch, and J. L. Pentecost, *J. Am. Ceram. Soc.*, 1985, **68**, C–285–C–286.

36. K.-C. Tsai, W.-F. Wu, C.-G. Chao, and C.-P. Kuan, *J. Electrochem. Soc.*, 2006, **153**, G492.

37. B. Zhou, H. Shi, X. D. Zhang, Q. Su, and Z. Y. Jiang, *J. Phys. D. Appl. Phys.*, 2014, **47**, 115502.

38. G. Scarel, S. Spiga, C. Wiemer, G. Tallarida, S. Ferrari, and M. Fanciulli, *Mater. Sci. Eng. B*, 2004, **109**, 11–16.

39. D. Min, N. Hoivik, G. U. Jensen, F. Tyholdt, C. Haavik, and U. Hanke, *Appl. Phys. A*, 2011, **105**, 867–874.

40. R. Mendoza-Reséndez, N. Núñez, E. Barriga-Castro, and C. Luna, *RSC Adv.*, 2013, **3**, 20765.

41. S. J. S. Qazi, A. R. Rennie, J. K. Cockcroft, and M. Vickers, *J. Colloid Interface Sci.*, 2009, **338**, 105–10.

42. Z. M. Rittersma, F. Roozeboom, M. a. Verheijen, J. G. M. van Berkum, T. Dao, J. H. M. Snijders, E. Vainonen-Ahlgren, E. Tois, M. Tuominen, and S. Haukka, *J. Electrochem. Soc.*, 2004, **151**, C716.

43. J. Yota, H. Shen, and R. Ramanathan, *J. Vac. Sci. Technol. A Vacuum, Surfaces, Film.*, 2013, **31**, 01A134.

44. R. Wu, B. Zhou, Q. Li, Z. Jiang, W. Wang, W. Ma, and X. Zhang, *J. Phys. D. Appl. Phys.*, 2012, **45**, 125304.

45. B.-K. Kim and H. Hamaguchi, *Mater. Res. Bull.*, 1997, **32**, 1367–1370.

46. M. M. Frank, S. Sayan, S. Dörmann, T. J. Emge, L. S. Wielunski, E. Garfunkel, and Y. J. Chabal, *Mater. Sci. Eng. B*, 2004, **109**, 6–10.

47. K. Tomida, K. Kita, and A. Toriumi, *Appl. Phys. Lett.*, 2006, **89**, 142902.

Journal of Materials Chemistry C Accepted Manuscript

48. D. A. Neumayer and E. Cartier, *J. Appl. Phys.*, 2001, **90**, 1801.

49. T. Hirata, *Phys. Rev. B. Condens. Matter*, 1994, **50**, 2874–2879.

50. M. Modreanu, J. Sancho-Parramon, O. Durand, B. Servet, M. Stchakovsky, C. Eypert, C. Naudin, a. Knowles, F. Bridou, and M.-F. Ravet, *Appl. Surf. Sci.*, 2006, **253**, 328–334.

51. D. Ceresoli and D. Vanderbilt, *Phys. Rev. B*, 2006, 74, 125108–6.

52. X. Zhao and D. Vanderbilt, *Phys. Rev. B*, 2002, **65**, 233106.

53. L. Koltunski and R. a. B. Devine, *Appl. Phys. Lett.*, 2001, **79**, 320.

54. R. Nyholm, A. Berndtsson, and N. Martensson, *J. Phys. C Solid …*, 1980, **13**, 1091.

55. D. D. Sarma and C. N. R. Rao, *J. Electron Spectros. Relat. Phenomena*, 1980, 20, 25–45.

56. L. Ramqvist, K. Hamrin, G. Johansson, A. Fahlman, and C. Nordling, *Solid State Commun.*, 1969, 7, v.

57. T. L. Barr, *J. Vac. Sci. Technol. A Vacuum, Surfaces, Film.*, 1995, **13**, 1239.

58. D. J. Miller, M. C. Biesinger, and N. S. McIntyre, *Surf. Interface Anal.*, 2002, **33**, 299–305.

59. M. Engelhard, J. Herman, R. Wallace, and D. Baer, *Surf. Sci. Spectra*, 2011, **18**, 46–57.

60. P. Dudek, R. Schmidt, M. Lukosius, G. Lupina, C. Wenger, a. Abrutis, M. Albert, K. Xu, and a. Devi, *Thin Solid Films*, 2011, **519**, 5796–5799.

61. T.-C. Tien, L.-C. Lin, L.-S. Lee, C.-J. Hwang, S. Maikap, and Y. M. Shulga, *J. Mater. Sci. Mater. Electron.*, 2009, **21**, 475–480.

62. J. P. Lehan, Y. Mao, B. G. Bovard, and H. A. Macleod, *Thin Solid Films*, 1991, 203, 227–250.

63. R. Smart, S. Mcintyre, and I. Bello, *Surf. Sci.*, 2011, 6, 86.

64. P. Steiner, H. Höchst, J. Schneider, S. Hüfner, and C. Politis, *Zeitschrift für Phys. B Condens. Matter Quanta*, 1979, **33**, 241–250.

65. Y. B. Yoo, J. H. Park, K. H. Lee, H. W. Lee, K. M. Song, S. J. Lee, and H. K. Baik, *J. Mater. Chem. C*, 2013, **1**, 1651.

66. P. Steiner and S. Hüfner, *Solid State Commun.*, 1982, 44, 1305–1307.

67. D. Barreca, A. Milanov, R. a. Fischer, A. Devi, and E. Tondello, *Surf. Sci. Spectra*, 2007, **14**, 34.

68. J. Aarik, H. Mändar, M. Kirm, and L. Pung, *Thin Solid Films*, 2004, **466**, 41–47.

69. T. Tan, Z. Liu, H. Lu, W. Liu, F. Yan, and W. Zhang, *Appl. Phys. A*, 2009, **97**, 475–479.

70. Y. Xie, Z. Ma, Y. Su, Y. Liu, L. Liu, H. Zhao, J. Zhou, Z. Zhang, J. Li, and E. Xie, *J. Mater. Res.*, 2011, 26, 50–54.

71. , P. Gonon, E. Gourvest, C. Dubarry, and E. Defay, *Appl. Phys. Lett.*, 2009, **94**, 253502.

72. A. Allan and et al., *INTERNATIONAL TECHNOLOGY ROADMAP FOR SEMICONDUCTORS*, 2012.

73. M. Lukosius, C. B. Kaynak, S. Rushworth, and C. Wenger, *J. Electrochem. Soc.*, 2011, **158**, G119.

74. - , S. Pasko, and C. Lohe, *J. Appl. Phys.*, 2008, **103**, 104103.

75. C. Wenger, M. Lukosius, G. Weidner, H.-J. Müssig, S. Pasko, and C. Lohe, *Thin Solid Films*, 2009, **517**, 6334–6336.

76. C. Zhu, H. Hu, X. Yu, S. J. Kim, A. Chin, M. F. Li, B. J. Cho, and D. L. Kwong, *IEDM*, 2003, **36**, 879–882.

77. J. Robertson, *Appl. Surf. Sci.*, 2002, **190**, 2–10.

Journal of Materials Chemistry C Accepted Manuscript

This journal is © The Royal Society of Chemistry 2012